Available online at www.sciencedirect.com
ScienceDirect
European Journal of Mechanics B/Fluids 26 (2007) 404–421

Interfacial capillary waves in the presence of electric fields

Scott Grandison [a], Demetrios T. Papageorgiou [b,*], Jean-Marc Vanden-Broeck [a]

[a] *School of Mathematics, University of East Anglia, Norwich NR4 7TJ, UK*
[b] *Department of Mathematical Sciences and Center for Applied Mathematics and Statistics, New Jersey Institute of Technology, University Heights, Newark, NJ 07102, USA*

Received 3 April 2006; received in revised form 14 June 2006; accepted 20 June 2006

Available online 8 September 2006

Abstract

Large amplitude capillary waves on an inviscid, incompressible fluid layer of density ρ_1 bounded by a second inviscid, incompressible fluid of density ρ_2 are computed in the presence of a uniform electric field acting in a direction parallel to the undisturbed configuration. Periodic travelling waves of arbitrary amplitudes and wavelengths are calculated and the effect of the electric field is studied. The solutions extend the results of Papageorgiou and Vanden-Broeck [D.T. Papageorgiou, J.-M. Vanden-Broeck, Large-amplitude capillary waves in electrified fluid sheets, J. Fluid Mech. 508 (2004) 71–88; D.T. Papageorgiou, J.-M. Vanden-Broeck, Antisymmetric capillary waves in electrified fluid sheets, Eur. J. Appl. Math. 16 (2004) 609–623] where the case of $\rho_2 = 0$ was treated. Fully nonlinear solutions are computed using boundary integral equation methods. It is shown that there are both symmetric and antisymmetric waves and their characteristics are explored and compared. When there is a jump in the undisturbed horizontal velocities, the flow is susceptible to Kelvin–Helmholtz instability. It is shown analytically in the linear regime, that even in the absence of surface tension, the flow is stabilized by sufficiently large electric fields. In such situations two wave speeds are possible for given electric fields and we construct these branches numerically when the amplitudes are not infinitesimal, both in the absence and presence of surface tension.

Keywords: Electrohydrodynamics; Liquid sheets; Travelling waves; Boundary integral methods

1. Introduction

Liquid sheets arise in many diverse physical and technological applications. Some of these include coating and curtain coating processes (as in, for example, photographic or magnetic membrane manufacture), where interfacial instabilities can affect the subsequent coating patterns and hence product quality (see Kistler and Schweizer [1] for a review). Liquid sheets are also used as liquid protector systems in inertial fusion energy reactor cavities—see Durbin et al. [2], [3] and the review by Abdel-Khalik and Yoda [4]. Another application is in float glass processes described by Warner [5,6]. An additional complication in liquid sheet dynamics is the possible rupture and formation of braids and droplets through primary and secondary instabilities. Such phenomena are mathematically challenging and find

* Corresponding author.
E-mail addresses: s.grandison@uea.ac.uk (S. Grandison), depapa@oak.njit.edu (D.T. Papageorgiou), j.vanden-broeck@uea.ac.uk (J.-M. Vanden-Broeck).

0997-7546/$ – see front matter
doi:10.1016/j.euromechflu.2006.06.005

applications in colloidal and bi-colloid systems, coalescence of emulsions, and fusion of lipid bi-layers or biological membranes—see for example Gallez and Prevost [7], Jain and Maldarelli [8], Maldarelli et al. [9], Maldarelli and Jain [10,11], and Prevost and Gallez [12].

The formation of waves on liquid layers when surface tension acts has been the subject of numerous investigations. Crapper [13] studied two-dimensional capillary waves in deep water and found a class of exact travelling wave solutions for which the interface can be a single or multi-valued function. When gravity is also present exact solutions are not possible. Gravity-capillary waves in irrotational fluids have been computed numerically by a number of authors including Schwartz and Vanden-Broeck [14], Chen and Saffman [15], Hogan [16], Hunter and Vanden-Broeck [17] and Grandison and Vanden-Broeck [18]. In all these investigations the surrounding regions are hydrodynamically passive, a restriction which we remove in the present work.

The full problem of wave formation on liquid sheets when an electric field acts has been studied by Papageorgiou and Vanden-Broeck [19,20]. No assumptions were made regarding the size of wave amplitudes and wavelengths, but the motion of the surrounding bounding fluid was neglected (the approximation is valid when the density of the outer fluid is very small compared to that of the inner fluid). Here, we develop a boundary integral equation technique where the fluid density ratio is a parameter and the motion of the second fluid is taken into account. We also note that the asymptotic long wave theories have also been developed to describe both the spatio-temporal evolution of the sheet as well as symmetric travelling waves supported on its surfaces (see Tilley et al. [21] and Papageorgiou and Vanden-Broeck [19] for inviscid flows and Savetasseranee et al. [22] for viscous flows). Excellent agreement between full numerics and asymptotics was found at wavelengths which are long compared to the undisturbed film thickness.

In the present study we consider waves propagating on the surface of a two-dimensional liquid layer, bounded by a second incompressible fluid, and in the presence of an electric field. The electric field acts in the plane of the sheet and is driven by a constant potential difference. For nonlinear interfacial deformations we must solve for the hydrodynamics and the electrostatics both inside and outside of the layer, the latter regions extending laterally to infinity. The hydrodynamics and electrostatics are coupled through the Maxwell stresses which modify the hydrodynamic stresses at the interface—see Jackson [23]. This constitutes a nonlinear problem which must, in general, be addressed numerically. We commence our study of the free-boundary problem by considering travelling wave solutions of arbitrary amplitude and wavelength. We will consider both symmetric and antisymmetric waves. There are different physical motivations for studying such waves: these include the use of electric fields in stabilizing the flow in parameter regimes where it can be unstable thus preventing or delaying rupture (see Tilley, Petropoulos and Papageorgiou [21] for such a calculation); electric fields can be used to form large amplitude travelling waves on interfaces (as calculated in the present work) and these can be of significant importance in heat and mass transfer enhancement—see Papageorgiou, Petropoulos and Vanden-Broeck [24] for references.

The paper is organized as follows. Section 2 describes the governing equations, gives the exact dimensionless problem and presents linearized dispersion relations for both the symmetric and anti-symmetric case. In Section 3 we analyze the linear problem in the presence of Kelvin–Helmholtz instability. Section 4 reformulates the symmetric and anti-symmetric problem in terms of integral equations. Section 5 presents a numerical scheme for the fully non-linear problem and Section 6 presents numerical results. In Section 7 we give our conclusions.

2. Governing equations

We consider the two-dimensional (a Cartesian coordinate system (x, y) is used) inviscid, incompressible and irrotational flow of a liquid of density ρ_1 occupying the region $\bar{S}(x,t) \leqslant y \leqslant S(x,t)$, $-\infty < x < \infty$, denoted by region 1. Schematics of the problem for symmetric and antisymmetric waves are depicted in Figs. 1 and 2, respectively. Surface tension of constant coefficient σ acts at the bounding interfaces, and a second inviscid, incompressible and irrotational fluid of density ρ_2 occupies the regions $y > S$, $y < \bar{S}$ (these are denoted by region 2). A uniform electric field given by $\mathbf{E}_0 = -(V_0/2L)\mathbf{i}$ is applied, where V_0 is the characteristic voltage drop over a characteristic distance, L; for example, L is a scale of separation of two electrodes placed perpendicular to the fluid layer and far apart. The fluids in regions 1 and 2 are taken to be perfect dielectrics with constant permittivities ε_1 and ε_2, respectively. An exact weak solution of the Euler equations exists given by $S = -\bar{S} = d$, $\mathbf{u}^{(1,2)} = c_{1,2}\mathbf{i}$, where $2d$ is constant representing the inner liquid layer thickness, while c_1 and c_2 represent constant, and generally different, horizontal velocities in regions 1 and 2 (appropriate constant pressures in regions 1 and 2 also follow—in the sequel subscripts or superscripts $1, 2$ denote variables in regions 1 and 2 respectively, unless otherwise stated). The electric field in this undisturbed configuration is

the same in regions 1 and 2 and is given by its applied value $\mathbf{E}_0 = -(V_0/2L)\mathbf{i}$. The model incorporates the competing physical effects of Kelvin–Helmholtz instability with surface tension and electric field dispersive regularizations (details are given later). It is of interest, therefore, to compute large amplitude travelling wave solutions governed by the full equations of motion and to evaluate their dependence on surface tension and electric field strength, for instance.

The mathematical problem can be stated in terms of the fluid potentials $\phi^{(1,2)}$ and electric potentials $V^{(1,2)}$. The corresponding velocity and electric fields are given by $\mathbf{u}^{(1,2)} = \nabla\phi^{(1,2)}$ and $\mathbf{E}^{(1,2)} = -\nabla V^{(1,2)}$ respectively. It is well known that for inviscid, incompressible, irrotational flows the fluid potentials are harmonic functions; this is also true for the voltage potentials in the present problem, since in the absence of charges in the bulk the displacement fields are solenoidal, namely $\nabla \cdot (\varepsilon_i \mathbf{E}^{(i)}) = 0$, $i = 1, 2$. The governing equations are:

$$\nabla^2\phi^{(1)} = \nabla^2 V^{(1)} = 0, \quad -\infty < x < \infty,\ \bar{S} < y < S,\ t > 0, \tag{2.1}$$

$$\nabla^2\phi^{(2)} = \nabla^2 V^{(2)} = 0, \quad -\infty < x < \infty,\ y < \bar{S},\ y > S,\ t > 0. \tag{2.2}$$

The conditions at infinity are

$$\phi_x^{(2)} = c_2, \quad V_x^{(2)} = \frac{V_0}{2L}, \quad \text{as } |y| \to \infty. \tag{2.3}$$

Even though the field equations above are linear, the problem is nonlinear due to the moving boundaries S and $\bar{S}$ which must also be determined as part of the solution. The boundary conditions at the free surfaces $y = S$ and $y = \bar{S}$ are the kinematic conditions (2.4) and (2.5), the continuity of the normal stresses (2.6), the continuity of the normal component of the displacement field (2.7), and the continuity of the tangential components of the electric field (2.8). These are at $y = S(x, t)$, for example,

$$S_t + \phi_x^{(1)} S_x - \phi_y^{(1)} = 0, \tag{2.4}$$

$$S_t + \phi_x^{(2)} S_x - \phi_y^{(2)} = 0, \tag{2.5}$$

$$[\mathbf{n} \cdot \mathbf{T} \cdot \mathbf{n}]_2^1 = \sigma \operatorname{div} \mathbf{n}, \tag{2.6}$$

$$[\varepsilon\, \mathbf{E} \cdot \mathbf{n}]_2^1 = 0, \tag{2.7}$$

$$[\mathbf{E} \cdot \mathbf{t}]_2^1 = 0, \tag{2.8}$$

where $[\cdot]_2^1$ denotes the jump in the quantity as the interface is crossed from regions 1 to 2. Similar equations are obtained for the antisymmetric case and are not included here for brevity. The vectors $\mathbf{n}$ and $\mathbf{t}$ are the outward-pointing normal and tangent to the interface respectively, and the stress tensor $\mathbf{T}$ is given by

$$T_{ij} = -p\delta_{ij} + \mathcal{E}_{ij}, \tag{2.9}$$

$$\mathcal{E}_{ij} = \epsilon\left(E_i E_j - \frac{1}{2}|\mathbf{E}|^2\delta_{ij}\right). \tag{2.10}$$

Here, p is the fluid pressure and δ_{ij} is the Kronecker delta. The stress tensor is composed of a hydrodynamic part and an electrical contribution $\mathcal{E}_{ij}$ known as the Maxwell stress tensor (see Jackson [23], for example). Analogous boundary conditions apply at the lower interface $y = \bar{S}$. In the Gauss law (2.7), we are assuming that the charge on the interface is zero a condition that is consistent with inviscid problems—charge variations along the interface induce tangential stresses which are balanced by viscous interfacial stresses. A boundary layer theory that can incorporate the presence of charges with an inviscid outer solution is the subject of current research.

2.1. Dimensionless equations

The equations and boundary conditions are made dimensionless using the typical horizontal length scale L and a typical velocity U. We write:

$$(x, y) = (Lx', Ly'), \quad S = LS', \quad t = \frac{L}{U}t',$$
$$\phi^{(1,2)} = LU\phi', \quad p^{(1,2)} = \rho_1 U^2 P^{(1,2)}, \quad V = V_0 V'. \tag{2.11}$$

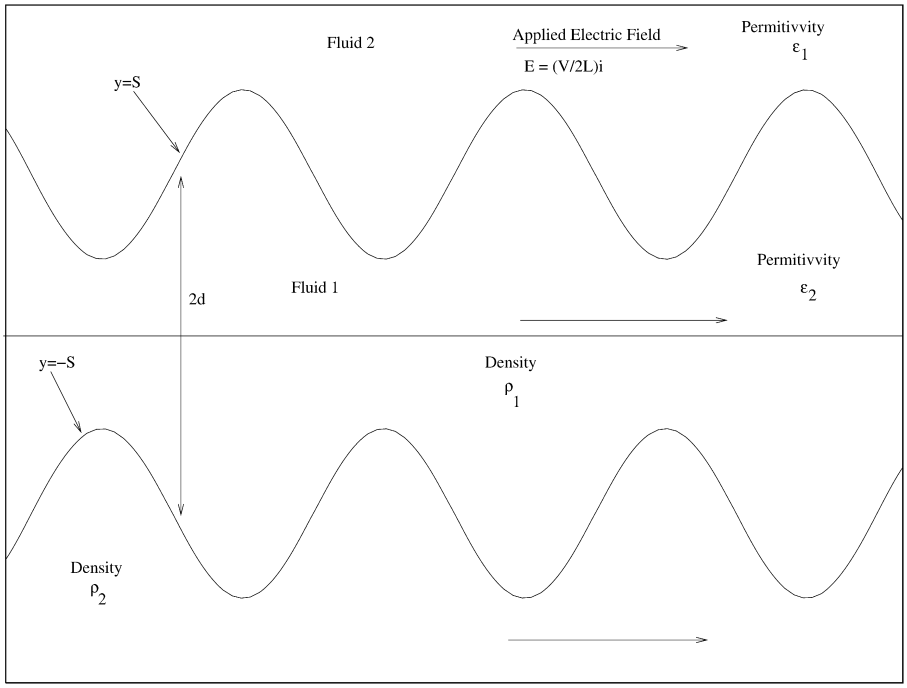

Fig. 1. Diagram showing a typical symmetric configuration.

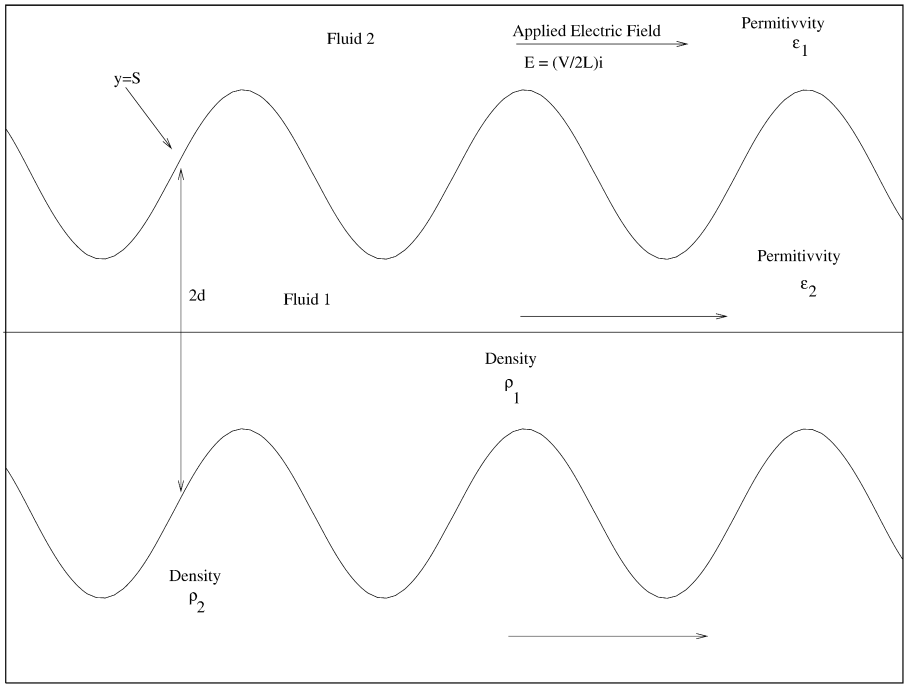

Fig. 2. Diagram showing a typical antisymmetric configuration.

We substitute the scalings (2.11) into the governing equations and interfacial conditions (2.4)–(2.8), and drop the primes. With this choice of reference scales the undisturbed interface is located at

$$y = d/L = \bar{d}. \tag{2.12}$$

The fluid and voltage potentials satisfy the Laplace equations (2.1), (2.2) with independent variables being dimensionless. The kinematic boundary conditions evaluated at $y = S(x,t)$ are also given by (2.4) and (2.5) in dimensionless variables, with similar conditions at $y = \bar{S}$.

The Bernoulli equations in regions 1 and 2 are

$$\phi_t^{(1)} + \frac{1}{2}\big(\phi_x^{(1)2} + \phi_y^{(1)2}\big) + P^{(1)} - B^{(1)} = 0, \tag{2.13}$$

$$\bar{\rho}\phi_t^{(2)} + \frac{\bar{\rho}}{2}\big(\phi_x^{(2)2} + \phi_y^{(2)2}\big) + P^{(2)} - B^{(2)} = 0, \tag{2.14}$$

where $B^{(1)}$ and $B^{(2)}$ are the Bernoulli constants. The dimensionless pressure jump $P^{(1)} - P^{(2)}$ is eliminated between (2.13) and (2.14) and the normal stress balance condition (2.6), to provide the following boundary condition that applies at $y = S$ (with an equivalent expression at $y = \bar{S}$):

$$\begin{aligned}\phi_t^{(1)} - \bar{\rho}\phi_t^{(2)} + \frac{1}{2}\big[\big(\phi_x^{(1)}\big)^2 + \big(\phi_y^{(1)}\big)^2\big] - \frac{\bar{\rho}}{2}\big[\big(\phi_x^{(2)}\big)^2 + \big(\phi_y^{(2)}\big)^2\big] \\ + \frac{E_b}{1+S_x^2}\left\{\frac{1}{2}\big(S_x^2 - 1\big)[\mathcal{M}_{11}]_2^1 - 2S_x[\mathcal{M}_{12}]_2^1\right\} - \frac{\tau S_{xx}}{(1+S_x^2)^{3/2}} - B_p = 0.\end{aligned} \tag{2.15}$$

The dimensionless parameters that appear in (2.15) are

$$\bar{\rho} = \frac{\rho_2}{\rho_1}, \quad E_b = \frac{\varepsilon_2 V_0^2}{\rho_1 U^2 L^2}, \quad \bar{\varepsilon} = \frac{\varepsilon_1}{\varepsilon_2}, \quad \tau = \frac{\sigma}{\rho_1 U^2 L}, \tag{2.16}$$

and represent the ratio of densities, an electric parameter measuring the ratio of electric to inertia forces (equivalent to an inverse electric Weber number), ratio of permittivities, and a surface tension parameter τ which is an inverse Weber number. The Bernoulli constant B_p follows from the undisturbed state and is given by $\bar{B}_p = \frac{1}{8}E_b(1-\bar{\varepsilon}) + \frac{1}{2}(U_1^2 - \bar{\rho}U_2^2)$, where $U_{1,2} = c_{1,2}/U$. The stress components in (2.15) are given by

$$\mathcal{M}_{11}^{(1,2)} = \left\{\frac{\varepsilon}{\varepsilon_2}\big[V_x^2 - V_y^2\big]\right\}^{(1,2)}, \tag{2.17}$$

$$\mathcal{M}_{12}^{(1,2)} = \left\{\frac{\varepsilon}{\varepsilon_2}[V_x V_y]\right\}^{(1,2)}. \tag{2.18}$$

Finally, the electric boundary conditions (2.7) and (2.8) become, in dimensionless variables,

$$\bar{\varepsilon}\big(V_y^{(1)} - S_x V_x^{(1)}\big) = V_y^{(2)} - S_x V_x^{(2)}, \tag{2.19}$$

$$V_x^{(1)} + S_x V_y^{(1)} = V_x^{(2)} + S_x V_y^{(2)}, \tag{2.20}$$

with analogous expressions at $y = \bar{S}$. The dimensionless far field conditions (2.3) become

$$\phi_x^{(2)} = U_2, \quad V_x^{(2)} = \frac{1}{2}, \quad \text{as } |y| \to \infty. \tag{2.21}$$

The voltage potential is symmetric with respect to the x-axis and we have $V_y^{(1)}(x,0,t) = 0$. The interfacial disturbances can be symmetric or antisymmetric. In the former case we have, for arbitrary amplitude solutions, $\phi_y^{(1)}(x,0,t) = 0$ and $\bar{S}(x,t) = -S(x,t)$. Antisymmetric solutions are straightforward in the linear regime and are also possible for arbitrary amplitude solutions as we show later in the numerical work of Section 6 (see also Papageorgiou and Vanden-Broeck [20]). The problem is completed with imposition of initial conditions.

The above system is nonlinear and, by analogy with nonlinear Kelvin–Helmholtz instability, the initial boundary value problem is not guaranteed to have solutions which exist globally in time when the surface tension is zero (see Krasny [25], for example). The addition of the electric field complicates the problem mathematically and it is of interest to consider its effects on solution properties and features. To obtain a basic understanding of the well-posedness of the initial value problem, we begin with a linear stability theory. This also allows the identification of parameter ranges where the presence of the electric field competes and indeed completely cancels Kelvin–Helmholtz instability (according to linear theory at least), even when surface tension is absent. One of our main objectives in

the present work is the numerical calculation of arbitrary amplitude travelling wave solutions and a description of their properties. The linear results are used to suggest their stability and a more complete study of the time-dependent problem is deferred for future work.

3. Linear theory

We consider linear stability properties of the dimensionless system given above. This can be achieved by writing

$$\phi^{(1)}(x,y,t) = U_1 x + \delta\hat{\phi}^{(1)}(y)\,\mathrm{e}^{i(kx-\omega t)} + \text{c.c.}, \tag{3.1}$$

$$\phi^{(2)}(x,y,t) = U_2 x + \delta\hat{\phi}^{(2)}(y)\,\mathrm{e}^{i(kx-\omega t)} + \text{c.c.}, \tag{3.2}$$

$$V^{(1)}(x,y,t) = \frac{1}{2}x + \delta\hat{V}^{(1)}(y)\,\mathrm{e}^{i(kx-\omega t)} + \text{c.c.}, \tag{3.3}$$

$$V^{(2)}(x,y,t) = \frac{1}{2}x + \delta\hat{V}^{(2)}(y)\,\mathrm{e}^{i(kx-\omega t)} + \text{c.c.}, \tag{3.4}$$

$$S(x,t) = d + \delta\hat{S}\,\mathrm{e}^{i(kx-\omega t)} + \text{c.c.}, \tag{3.5}$$

where $\delta \ll 1$ is a linearization parameter and c.c. denotes complex conjugates. It is sufficient to study symmetric and antisymmetric perturbations characterized by $\hat{\phi}_y^{(1)}(0) = \hat{V}^{(1)}(0) = 0$ and $\hat{\phi}^{(1)}(0) = \hat{V}^{(1)}(0) = 0$, respectively. The boundary conditions at infinity are

$$\hat{\phi}^{(2)},\ \hat{V}^{(2)} \to 0, \quad \text{as } y \to \infty. \tag{3.6}$$

A dispersion relation is found by substituting (3.1)–(3.5) into the governing equations (2.1)–(2.2) and interfacial boundary conditions (2.4), (2.5), (2.15), (2.19) and (2.20), linearizing with respect to δ and applying either symmetric or antisymmetric velocity perturbation conditions. The eigenfunctions are $\hat{\phi}^{(2)} = \mathrm{e}^{-|k|y}$, $\hat{V}^{(2)} = \mathrm{e}^{-|k|y}$, and, either $\hat{\phi}^{(1)} = \cosh ky$ and $\hat{V}^{(1)} = \cosh ky$ for symmetric perturbations, or $\hat{\phi}^{(1)} = \sinh ky$, $\hat{V}^{(1)} = \sinh ky$ for antisymmetric ones. The result is

$$(\omega - kU_1)^2 + \bar{\rho}\big|\tanh(kd)\big|(\omega - kU_2)^2 - \frac{(1-\bar{\varepsilon})^2 E_b}{4}\frac{k^3\tanh kd}{|k| + \bar{\varepsilon}k\tanh kd} - \tau k^3\tanh kd = 0, \tag{3.7}$$

and

$$(\omega - kU_1)^2 + \bar{\rho}\big|\coth(kd)\big|(\omega - kU_2)^2 - \frac{(1-\bar{\varepsilon})^2 E_b}{4}\frac{k^3\coth kd}{|k| + \bar{\varepsilon}k\coth kd} - \tau k^3\coth kd = 0, \tag{3.8}$$

for symmetric and antisymmetric modes, respectively.

The dispersion relations (3.7) and (3.8) contain the effects of electric fields, Kelvin–Helmholtz instability and surface tension regularization of short waves. In what follows we analyze certain limits in order to evaluate the relative effect of the different physical mechanisms present. For brevity we consider the symmetric case, unless otherwise stated.

3.1. Equal stream velocities

In this case the two background stream velocities are constant and equal, say $U_1 = U_2 = c_s$. This in turn implies that the Kelvin–Helmholtz instability mechanism is absent and we expect dispersive waves when surface tension is also present. Indeed, it follows from (3.7) and (3.8) that ω is real and linear dispersive waves are generated. The expressions are

$$(\omega - kc_s)^2 = \left[\frac{E_b}{4}(1-\varepsilon)^2\frac{k^3\tanh kd}{\varepsilon k\tanh kd + |k|} + \tau k^3\tanh kd\right](1 + \bar{\rho}\tanh kd)^{-1}, \tag{3.9}$$

and

$$(\omega - kc_s)^2 = \left[\frac{E_b}{4}(1-\varepsilon)^2\frac{k^3\coth kd}{\varepsilon k\coth kd + |k|} + \tau k^3\coth kd\right](1 + \bar{\rho}\coth kd)^{-1} \tag{3.10}$$

for symmetric and antisymmetric modes respectively. It is seen that without loss of generality we can set $c_s \equiv 0$ by applying a Galilean transformation. The two roots produce right- and left-moving waves and without loss of generality we compute right-moving ones in the numerical work that follows. In the further limit where the upper fluid is absent ($\bar{\rho} = 0$) we recover the results of Papageorgiou and Vanden-Broeck [19] for symmetric waves and Papageorgiou and Vanden-Broeck [20] for antisymmetric ones. The calculation of arbitrary amplitude and wavelength nonlinear travelling waves carried out in the present work, extends the work of [19,20] by including a second surrounding flow.

3.2. Unequal stream velocities

For unequal unperturbed stream velocities the flow is susceptible to the Kelvin–Helmholtz instability. It is of interest here to evaluate the effect of the electric field on this instability when surface tension is absent or present. As shown next, for sufficiently large values of E_b, the Kelvin–Helmholtz instability is completely stabilized and hence the electric field acts as a lower order dispersive regularization as compared to the regularization provided by surface tension. The dispersion relations (3.7) and (3.8) can be written as:

$$\left(\frac{\omega}{k} - \frac{U_1 + U_2\bar{\rho}|\tanh kd|}{1+\bar{\rho}|\tanh kd|}\right)^2 + \frac{\bar{\rho}|\tanh kd|}{(1+\bar{\rho}|\tanh kd|)^2}(U_1 - U_2)^2 - \frac{(1-\bar{\varepsilon})^2 E_b}{4}\frac{k\tanh kd}{(|k| + \bar{\varepsilon}k\tanh kd)(1+\bar{\rho}|\tanh kd|)} - \frac{\tau k\tanh kd}{1+\bar{\rho}|\tanh kd|} = 0, \tag{3.11}$$

$$\left(\frac{\omega}{k} - \frac{U_1 + U_2\bar{\rho}|\coth kd|}{1+\bar{\rho}|\coth kd|}\right)^2 + \frac{\bar{\rho}|\coth kd|}{(1+\bar{\rho}|\coth kd|)^2}(U_1 - U_2)^2 - \frac{(1-\bar{\varepsilon})^2 E_b}{4}\frac{k\coth kd}{(|k| + \bar{\varepsilon}k\coth kd)(1+\bar{\rho}|\coth kd|)} - \frac{\tau k\coth kd}{1+\bar{\rho}|\coth kd|} = 0. \tag{3.12}$$

For *instability* we require ω to be complex (the roots come in a conjugate pair, one of which is stable and the other unstable). For symmetric modes this happens if

$$\mathcal{D}_1 = -\frac{(U_1 - U_2)^2\bar{\rho}|\tanh kd|}{1+\bar{\rho}|\tanh kd|} + \frac{E_b(1-\bar{\varepsilon})^2 k\tanh kd}{4(|k| + \bar{\varepsilon}k\tanh kd)} + \tau k\tanh kd < 0, \tag{3.13}$$

and for antisymmetric modes the condition for instability becomes

$$\mathcal{D}_2 = -\frac{(U_1 - U_2)^2\bar{\rho}|\coth kd|}{1+\bar{\rho}|\coth kd|} + \frac{E_b(1-\bar{\varepsilon})^2 k\coth kd}{4(|k| + \bar{\varepsilon}k\coth kd)} + \tau k\coth kd < 0, \tag{3.14}$$

It follows from conditions (3.13), (3.14) that when $\tau \neq 0$, instability is impossible for sufficiently large k (for large k the surface tension term is $\mathcal{O}(k^3)$ and positive while all other terms are $\mathcal{O}(k^2)$, invalidating the conditions for instability). This is expected since surface tension acts to dispersively regularize short waves. Considering (3.13) first, it is possible to obtain a bound for the band of unstable waves by noting that as k varies, instability is guaranteed when $\max_k\{\mathcal{D}_1\} < 0$. After some algebra this leads to the following bound for the unstable symmetric wave numbers (note that $\mathcal{D}_{1,2}$ are even functions of k):

$$|k| < \frac{4\bar{\rho}(U_1 - U_2)^2 - (1+\bar{\rho})E_b(1-\bar{\varepsilon})^2}{4\tau(1+\bar{\rho})}. \tag{3.15}$$

Clearly, a sufficient condition for instability (the bound is not exact) is

$$E_b < E_{bc} = \frac{4\bar{\rho}(U_1 - U_2)^2}{(1+\bar{\rho})(1-\bar{\varepsilon})^2}, \tag{3.16}$$

which can be satisfied if E_b is made sufficiently small, for example, all other parameters held fixed. If $\tau = 0$, the flow is unstable if (3.16) is satisfied and stable if $E_b > E_{bc}$. The growth rates (when unstable) are proportional to k as is usual in Kelvin–Helmholtz instability. These results are also easily established by considering the large k behavior of (3.11) and (3.12) for $\tau = 0$, and yields, for both symmetric and antisymmetric modes,

$$\frac{\omega}{k} = \frac{U_1 + \bar{\rho}U_2}{1+\bar{\rho}} \pm \sqrt{\frac{(1-\bar{\varepsilon})^2 E_b}{4(1+\bar{\varepsilon})(1+\bar{\rho})} - \frac{\bar{\rho}(U_1 - U_2)^2}{(1+\bar{\rho})^2}}. \tag{3.17}$$

It is seen, then, that when E_b is large enough, ω is real and proportional to k so that short linear waves translate with a uniform speed which varies as the square root of E_b. If, on the other hand, E_b is sufficiently small, then ω is imaginary and linear short waves grow exponentially fast according to $\exp(|\omega_i(k)|t)$, where we define $\omega = \omega_r + i\omega_i$ and use (3.17) at large k. This growth is structurally identical to Kelvin–Helmholtz instability and the nonlinear initial value problem is consequently ill-posed. The bound (3.16) is consistent with this large k result. It is also seen that to stabilize faster flows (large c) we need larger values of E_b, the increase being quadratic in $(U_1 - U_2)$.

For general values of the parameters, stability or instability is easily deduced from (3.11) and (3.12) by finding the values of k such that $\omega_i(k) \neq 0$. In situations where $E_b > E_{bc}$, the behavior is dispersive and there are two real values for ω and hence two possible wave speeds. The linear results are used to guide our calculations of arbitrary amplitude travelling waves and we will calculate solutions when surface tension is present or absent and for sufficiently large E_b so that the Kelvin–Helmholtz instability is absent (linearly at least).

4. Reformulation as integral equations

Here we will adopt a similar approach to Papageorgiou and Vanden-Broeck [19,20]. The main difference will be the introduction of integral equations for $\phi^{(2)}$. Some of the details are repeated for the sake of completeness.

We consider a train of waves of wavelength λ travelling at a constant velocity c in a two-fluid system. Precise definitions of c and the thickness will be given later. We choose a frame of reference in which the flow is steady and we introduce Cartesian co-ordinates with the x-axis parallel to the undisturbed state and the origin at the centreline. The line of symmetry/antisymmetry is then at $y = 0$. For symmetric waves

$$\bar{S}(x) = -S(x), \tag{4.1}$$

$$\phi^{(1,2)}(x, \bar{S}) = \phi^{(1,2)}(x, S), \tag{4.2}$$

and

$$V^{(1,2)}(x, \bar{S}) = V^{(1,2)}(x, S). \tag{4.3}$$

For antisymmetric waves

$$\bar{S}(x) = -S\left(\frac{\pi\lambda}{2} + x\right), \tag{4.4}$$

$$\phi^{(1,2)}(x, \bar{S}) = \phi^{(1,2)}\left(\frac{\pi\lambda}{2} + x, S\right), \tag{4.5}$$

and

$$V^{(1,2)}(x, \bar{S}) = V^{(1,2)}\left(\frac{\pi\lambda}{2} + x, S\right). \tag{4.6}$$

We describe the free surface $y = S(x)$ parametrically by $x = X(s)$ and $y = Y(s)$ where s is the arc length, implying that

$$X'^2(s) + Y'^2(s) = 1. \tag{4.7}$$

We choose $x = s = 0$ at a crest and express $X(s)$ and $Y(s)$ in terms of $X'(s)$ and $Y'(s)$ as

$$X(s) = \int_0^s X'(r)\,\mathrm{d}r, \tag{4.8}$$

$$Y(s) = \alpha + \int_0^2 Y'(r)\,\mathrm{d}r. \tag{4.9}$$

Here α is the ordinate of the crests.

Next we rewrite (2.15) in the new frame of reference as

$$\frac{1}{2}\left[\left(\phi_x^{(1)}\right)^2+\left(\phi_y^{(1)}\right)^2\right]-\frac{\bar{\rho}}{2}\left[\left(\phi_x^{(2)}\right)^2+\left(\phi_y^{(2)}\right)^2\right]+\frac{E_b}{1+S_x^2}\left\{\frac{1}{2}\left(S_x^2-1\right)[\mathcal{M}_{11}]_2^1-2S_x[\mathcal{M}_{12}]_2^1\right\}$$
$$=Y''(s)X'(s)-X''(s)Y'(s)+B \tag{4.10}$$

where B is a constant to be found as part of the solution. Eq. (4.10) reduces to Eq. (3.4) of Papageorgiou and Vanden-Broeck [19] when $\bar{\rho}=0$.

The horizontal and vertical components of the velocity in the two fluids are given by

$$u^{(1,2)}=\frac{\partial\phi^{(1,2)}}{\partial x}, \tag{4.11}$$

$$v^{(1,2)}=\frac{\partial\phi^{(1,2)}}{\partial y}. \tag{4.12}$$

We define the depth as the ordinate of the mean level of the interface. Therefore, we impose

$$\int_0^b Y(s)X'(s)\,\mathrm{d}s=\bar{d}, \tag{4.13}$$

where b is the length of a periodic interfacial wave. We also define the velocity c as the average horizontal velocity at a constant level of y within fluid 1. Thus we write

$$c=\frac{1}{\lambda}\int_0^\lambda u\,\mathrm{d}x, \tag{4.14}$$

where y is taken at a constant level. The irrotationality of the flow in region 1 implies that the value of c is independent of the constant level of y chosen provided it is in fluid 1. The irrotationality of the flow implies also that (4.14) can be rewritten as

$$c=\frac{1}{\lambda}\int_0^b\left[u^{(1)}X'(s)+v^{(1)}Y'(s)\right]\mathrm{d}s. \tag{4.15}$$

The relative velocity $\bar{c}$ of fluids 1 and 2 is defined as the difference in the fluid speed between the fluid jet and the bounding fluid. Therefore we have

$$\bar{c}=\frac{1}{\lambda}\left\{\int_0^b\left[u^{(1)}X'(s)+v^{(1)}Y'(s)\right]\mathrm{d}s-\int_0^b\left[u^{(2)}X'(s)+v^{(2)}Y'(s)\right]\mathrm{d}s\right\}. \tag{4.16}$$

As $y\to\infty$, $V_x^{(2)}$ approaches $1/2$, and since $V^{(2)}$ satisfies Laplace's equation, we have

$$\int_0^b\left[V_x^{(2)}X'(s)+V_y^{(2)}Y'(s)\right]\mathrm{d}s=\int_0^\lambda V_x^{(2)}\,\mathrm{d}x \tag{4.17}$$

where the integral on the right-hand side is taken at a constant y. Taking the limit as this constant approaches infinity we obtain

$$\frac{1}{\lambda}\int_0^b\left[V_x^{(2)}X'(s)+V_y^{(2)}Y'(s)\right]\mathrm{d}s=\frac{1}{2}. \tag{4.18}$$

Next we map the fluid in region 1 within $-\lambda/2<x<\lambda/2$ from the $(z=x+iy)$-plane into the interior of an annular region of the ζ-plane by the transformation

$$\zeta^{(1)}=\exp(-2i\pi z/\lambda). \tag{4.19}$$

Similarly we map the fluid in region 2 to the interior of a unit circle by the transformation

$$\zeta^{(2)} = \exp(2i\pi z/\lambda). \tag{4.20}$$

Applying Cauchy's integral equation formula to the functions $W^{(1,2)} = u^{(1,2)} - iv^{(1,2)}$ and $V_x^{(1,2)} - iV_y^{(1,2)}$ in the annular region of the $\zeta^{(1)}$-plane and the circular region of the $\zeta^{(2)}$ plane yields expressions for $u^{(1)}$, $u^{(2)}$, $V_x^{(1)}$ and $V_x^{(2)}$. Our integral representations for $u^{(1)}$, $V_x^{(1)}$ and $V_x^{(2)}$ are identical to those derived by Papageorgiou and Vanden-Broeck [19] in the case of symmetric waves and Papageorgiou and Vanden-Broeck [20] in the case of antisymmetric waves.

4.1. Symmetric integral equations

Let $\beta = 2\pi/\lambda$, $V_1 = u(s)X'(s) + v(s)Y'(s)$, $V_2 = u(s)Y'(s) - v(s)X'(s)$, $Y_\pm = Y(r) \pm Y(s)$ and $X_\pm = X(r) \pm X(s)$. Papageorgiou and Vanden-Broeck [19] derived the following integral equations by using Cauchy's integral equation formula

$$\begin{aligned}
\frac{\lambda}{2}u^{(1)}(r) = &\int_0^{b/2} \frac{V_1(1 - e^{\beta Y_-}\cos(\beta X_+)) - V_2(e^{\beta Y_-}\sin(\beta X_+))}{1 + e^{2\beta Y_-} - 2e^{\beta Y_-}\cos(\beta X_+)}\,ds \\
&+ \int_0^{b/2} \frac{V_1(1 - e^{\beta Y_-}\cos(\beta X_-)) - V_2(e^{\beta Y_-}\sin(\beta X_-))}{1 + e^{2\beta Y_-} - 2e^{\beta Y_-}\cos(\beta X_-)}\,ds \\
&- \int_0^{b/2} \frac{V_1(1 - e^{\beta Y_+}\cos(\beta X_-)) - V_2(e^{\beta Y_+}\sin(\beta X_-))}{1 + e^{2\beta Y_+} - 2e^{\beta Y_+}\cos(\beta X_-)}\,ds \\
&- \int_0^{b/2} \frac{V_1(1 - e^{\beta Y_+}\cos(\beta X_+)) - V_2(e^{\beta Y_+}\sin(\beta X_+))}{1 + e^{2\beta Y_+} - 2e^{\beta Y_+}\cos(\beta X_+)}\,ds,
\end{aligned} \tag{4.21}$$

$$\begin{aligned}
\frac{\lambda}{2}V_x^{(1)}(r) = &\int_0^{b/2} \frac{A_1(1 - e^{\beta Y_-}\cos(\beta X_+)) - A_2(e^{\beta Y_-}\sin(\beta X_+))}{1 + e^{2\beta Y_-} - 2e^{\beta Y_-}\cos(\beta X_+)}\,ds \\
&+ \int_0^{b/2} \frac{A_1(1 - e^{\beta Y_-}\cos(\beta X_-)) - A_2(e^{\beta Y_-}\sin(\beta X_-))}{1 + e^{2\beta Y_-} - 2e^{\beta Y_-}\cos(\beta X_-)}\,ds \\
&- \int_0^{b/2} \frac{A_1(1 - e^{\beta Y_+}\cos(\beta X_-)) - A_2(e^{\beta Y_+}\sin(\beta X_-))}{1 + e^{2\beta Y_+} - 2e^{\beta Y_+}\cos(\beta X_-)}\,ds \\
&- \int_0^{b/2} \frac{A_1(1 - e^{\beta Y_+}\cos(\beta X_+)) - A_2(e^{\beta Y_+}\sin(\beta X_+))}{1 + e^{2\beta Y_+} - 2e^{\beta Y_+}\cos(\beta X_+)}\,ds.
\end{aligned} \tag{4.22}$$

Here $A_1 = V_x^{(1)}(s)X'(s) + V_y^{(1)}(s)Y'(s)$ and $A_2 = V_x^{(1)}(s)Y'(s) - V_y^{(1)}(s)X'(s)$. In addition,

$$\begin{aligned}
V_x^{(2)} = &\frac{2}{\lambda}\,\mathrm{Im}\int_0^b \frac{(V_x^{(2)} - iV_y^{(2)})(iX'(s) - Y'(s))}{1 - \exp(\frac{2i\pi}{\lambda}(X(t) - X(s)) - \frac{2\pi}{\lambda}(Y(t) - Y(s)))}\,ds \\
&+ \frac{2}{\lambda}\mathrm{Im}\int_0^b \frac{(V_x^{(2)} + iV_y^{(2)})(iX'(s) + Y'(s))}{1 - \exp(\frac{2i\pi}{\lambda}(X(t) + X(s)) - \frac{2\pi}{\lambda}(Y(t) - Y(s)))}\,ds.
\end{aligned} \tag{4.23}$$

Following the analysis in [19] we can derive the additional integral equation for the outer flow

$$u^{(2)} = \frac{2}{\lambda}\mathrm{Im}\int_0^b \frac{(u^{(2)} - iv^{(2)})(iX'(s) - Y'(s))}{1 - \exp(\frac{2i\pi}{\lambda}(X(t) - X(s)) - \frac{2\pi}{\lambda}(Y(t) - Y(s)))}\,\mathrm{d}s + \frac{2}{\lambda}\mathrm{Im}\int_0^b \frac{(u^{(2)} + iv^{(2)})(iX'(s) + Y'(s))}{1 - \exp(\frac{2i\pi}{\lambda}(X(t) + X(s)) - \frac{2\pi}{\lambda}(Y(t) - Y(s)))}\,\mathrm{d}s. \tag{4.24}$$

4.2. Antisymmetric integral equations

In addition to the definitions in Section 4.1 we also define $\tilde{V}_1 = u(\frac{b}{2} - s)X'(\frac{b}{2} - s) + v(\frac{b}{2} - s)Y'(\frac{b}{2} - s)$, $\tilde{V}_2 = u(\frac{b}{2} - s)Y'(\frac{b}{2} - s) - v(\frac{b}{2} - s)X'(\frac{b}{2} - s)$, $\tilde{Y}_\pm = Y(r) \pm Y(\frac{b}{2} - s)$, $\tilde{X}_\pm = X(r) \pm [\frac{\lambda}{2} - X(\frac{b}{2} - s)]$, $\tilde{A}_1 = V_x^{(2)}(\frac{b}{2} - s)X'(\frac{b}{2} - s) + V_y^{(1)}(\frac{b}{2} - s)Y'(\frac{b}{2} - s)$ and $\tilde{A}_2 = V_x^{(1)}(\frac{b}{2} - s)Y'(\frac{b}{2} - s) - V_y^{(1)}(\frac{b}{2} - s)X'(\frac{b}{2} - s)$. Papageorgiou and Vanden-Broeck [19] derived the following integral equations using Cauchy's integral equation formula for the antisymmetric case:

$$\begin{aligned}\frac{\lambda}{2}u^{(1)}(r) = {} & \int_0^{b/2} \frac{V_1(1 - \mathrm{e}^{\beta Y_-}\cos(\beta X_+)) - V_2(\mathrm{e}^{\beta Y_-}\sin(\beta X_+))}{1 + \mathrm{e}^{2\beta Y_-} - 2\mathrm{e}^{\beta Y_-}\cos(\beta X_+)}\,\mathrm{d}s \\ & + \int_0^{b/2} \frac{V_1(1 - \mathrm{e}^{\beta Y_-}\cos(\beta X_-)) - V_2(\mathrm{e}^{\beta Y_-}\sin(\beta X_-))}{1 + \mathrm{e}^{2\beta Y_-} - 2\mathrm{e}^{\beta Y_-}\cos(\beta X_-)}\,\mathrm{d}s \\ & - \int_0^{b/2} \frac{\tilde{V}_1(1 - \mathrm{e}^{\beta \tilde{Y}_+}\cos(\beta \tilde{X}_-)) - \tilde{V}_2(\mathrm{e}^{\beta \tilde{Y}_+}\sin(\beta \tilde{X}_-))}{1 + \mathrm{e}^{2\beta \tilde{Y}_+} - 2\mathrm{e}^{\beta \tilde{Y}_+}\cos(\beta \tilde{X}_-)}\,\mathrm{d}s \\ & - \int_0^{b/2} \frac{\tilde{V}_1(1 - \mathrm{e}^{\beta \tilde{Y}_+}\cos(\beta \tilde{X}_+)) - \tilde{V}_2(\mathrm{e}^{\beta \tilde{Y}_+}\sin(\beta \tilde{X}_+))}{1 + \mathrm{e}^{2\beta \tilde{Y}_+} - 2\mathrm{e}^{\beta \tilde{Y}_+}\cos(\beta \tilde{X}_+)}\,\mathrm{d}s,\end{aligned} \tag{4.25}$$

$$\begin{aligned}\frac{\lambda}{2}V_x^{(1)}(r) = {} & \int_0^{b/2} \frac{A_1(1 - \mathrm{e}^{\beta Y_-}\cos(\beta X_+)) - A_2(\mathrm{e}^{\beta Y_-}\sin(\beta X_+))}{1 + \mathrm{e}^{2\beta Y_-} - 2\mathrm{e}^{\beta Y_-}\cos(\beta X_+)}\,\mathrm{d}s \\ & + \int_0^{b/2} \frac{A_1(1 - \mathrm{e}^{\beta Y_-}\cos(\beta X_-)) - A_2(\mathrm{e}^{\beta Y_-}\sin(\beta X_-))}{1 + \mathrm{e}^{2\beta Y_-} - 2\mathrm{e}^{\beta Y_-}\cos(\beta X_-)}\,\mathrm{d}s \\ & - \int_0^{b/2} \frac{\tilde{A}_1(1 - \mathrm{e}^{\beta \tilde{Y}_+}\cos(\beta \tilde{X}_-)) - \tilde{A}_2(\mathrm{e}^{\beta \tilde{Y}_+}\sin(\beta \tilde{X}_-))}{1 + \mathrm{e}^{2\beta \tilde{Y}_+} - 2\mathrm{e}^{\beta \tilde{Y}_+}\cos(\beta \tilde{X}_-)}\,\mathrm{d}s \\ & - \int_0^{b/2} \frac{\tilde{A}_1(1 - \mathrm{e}^{\beta \tilde{Y}_+}\cos(\beta \tilde{X}_+)) - \tilde{A}_2(\mathrm{e}^{\beta \tilde{Y}_+}\sin(\beta \tilde{X}_+))}{1 + \mathrm{e}^{2\beta \tilde{Y}_+} - 2\mathrm{e}^{\beta \tilde{Y}_+}\cos(\beta \tilde{X}_+)}\,\mathrm{d}s,\end{aligned} \tag{4.26}$$

$$V_x^{(2)} = \frac{2}{\lambda}\,\mathrm{Im}\int_0^b \frac{(V_x^{(2)} - iV_y^{(2)})(iX'(s) - Y'(s))}{1 - \exp(\frac{2i\pi}{\lambda}(X(t) - X(s)) - \frac{2\pi}{\lambda}(Y(t) - Y(s)))}\,\mathrm{d}s + \frac{2}{\lambda}\,\mathrm{Im}\int_0^b \frac{(V_x^{(2)} + iV_y^{(2)})(iX'(s) + Y'(s))}{1 - \exp(\frac{2i\pi}{\lambda}(X(t) + X(s)) - \frac{2\pi}{\lambda}(Y(t) - Y(s)))}\,\mathrm{d}s. \tag{4.27}$$

Note that Eqs. (4.26)–(4.27) in the outer region 2 are the same as the corresponding ones (4.23)–(4.24) for the symmetric waves. Again we obtain one further integral expression for $u^{(2)}$ using Cauchy's integral equation

$$u^{(2)} = \frac{2}{\lambda}\,\mathrm{Im}\int_0^b \frac{(u^{(2)} - iv^{(2)})(iX'(s) - Y'(s))}{1 - \exp(\frac{2i\pi}{\lambda}(X(t) - X(s)) - \frac{2\pi}{\lambda}(Y(t) - Y(s)))}\,\mathrm{d}s + \frac{2}{\lambda}\,\mathrm{Im}\int_0^b \frac{(u^{(2)} + iv^{(2)})(iX'(s) + Y'(s))}{1 - \exp(\frac{2i\pi}{\lambda}(X(t) + X(s)) - \frac{2\pi}{\lambda}(Y(t) - Y(s)))}\,\mathrm{d}s. \tag{4.28}$$

4.3. Further expressions

We also write $V_x^{(1)}$ and $V_y^{(1)}$ in terms of $V_x^{(2)}$ and $V_y^{(2)}$ by using (2.19) and (2.20)

$$V_x^{(1)} = \frac{1}{1+S_x^2}\left[V_y^{(2)}\left(S_x - \frac{S_x}{\bar{\varepsilon}}\right) + V_x^{(2)}\left(1 + \frac{S_x^2}{\bar{\varepsilon}}\right)\right], \tag{4.29}$$

$$V_y^{(1)} = \frac{1}{1+S_x^2}\left[V_y^{(2)}\left(S_x^2 + \frac{1}{\bar{\varepsilon}}\right) + V_x^{(2)}\left(S_x - \frac{S_x}{\bar{\varepsilon}}\right)\right]. \tag{4.30}$$

Finally the kinematic boundary conditions on the interface give

$$u^{(1)}Y'(s) - v^{(1)}X'(s) = 0, \tag{4.31}$$

$$u^{(2)}Y'(s) - v^{(2)}X'(s) = 0. \tag{4.32}$$

We also define the amplitude, h, as

$$h = Y(0) - Y\left(\frac{1}{2}b\right). \tag{4.33}$$

We now seek eight functions $X'(s)$, $Y'(s)$, $u^{(1)}$, $v^{(1)}$, $u^{(2)}$, $v^{(2)}$, $V_x^{(2)}$, $V_y^{(2)}$ and three parameters α, B and b satisfying (4.8)–(4.10), (4.21) (or (4.25)), (4.22) (or (4.26)), (4.23) (or (4.27)), (4.24) (or (4.28)–(4.32) and (4.33). These equations are next solved numerically.

5. Numerical method

We define equally spaced mesh points over the interval $[0, \frac{1}{2}b]$ by the formulae

$$s_I = \frac{b}{2(N-1)}(I-1), \quad I = 1, \ldots, N, \tag{5.1}$$

$$s_{I+1/2} = \frac{(s_{I+1} + s_I)}{2}, \quad I = 1, \ldots, N. \tag{5.2}$$

We also introduce the $8N$ unknowns $X_I' = X'(s_I)$, $Y_I' = Y'(s_I)$, $u_I^{(1)} = u^{(1)}(s_I)$, $v_I^{(1)} = v^{(1)}(s_I)$, $u_I^{(2)} = u^{(2)}(s_I)$, $v_I^{(2)} = v^{(2)}(s_I)$, $V_x^I = V_x^{(2)}(s_I)$, $V_y^I = V_y^{(2)}(s_I)$.

We satisfy (4.7), (4.10), (4.31) and (4.32) at the mesh points (5.1). This leads to $4N$ equations. $2N-4$ equations are obtained by satisfying (4.21) (or (4.25)) at the mesh points (5.2), $I = 1, \ldots, N-2$, and (4.22) (or (4.26)) at the mesh points (5.2), $I = 2, \ldots, N-1$. The integrals in (4.21) (or (4.25)) and (4.22) (or (4.26)) are approximated using the trapezoidal rule with a summation over the mesh points (5.1). The symmetry of the quadrature and of the discretization enables us to evaluate the Cauchy principal values as if they were ordinary integrals. Similarly we satisfy (4.23) (or (4.27)) and (4.24) (or (4.28)) at the mesh points (5.1), $I = 1, \ldots, N-1$ with a summation over the mesh points (5.2). Eight more equations are obtained by setting $v_1^{(1)} = v_N^{(1)} = V_y^1 = V_y^N = 0$, $X(n) = \lambda/2$ and by imposing (4.13) and (4.18). One more equation is given by (4.33) with h prescribed. The last equation is obtained from (4.16) with $\bar{c}$ set to zero. This gives a system of $8N+3$ nonlinear algebraic equations for the $8N+3$ unknowns, B, b, α and X_I', Y_I', $u_I^{(1)}$, $v_I^{(1)}$, $u_I^{(2)}$, $v_I^{(2)}$, V_x^I, V_y^I, $I = 1, \ldots, N$. This system is solved by Newton's method.

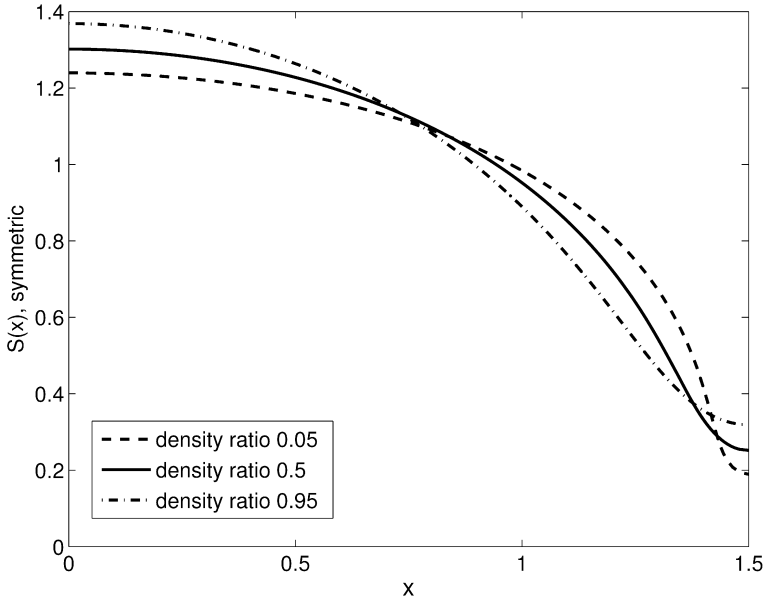

Fig. 3. Symmetric wave results for $E_b = 3$, $\bar{\varepsilon} = 0.075$, $\lambda = 3.0$, $h = 1.05$, $\bar{d} = 1.0$. The dashed line represents the free-surface when $\bar{\rho} = 0.05$, the solid line is for $\bar{\rho} = 0.5$ and the dash-dot line is $\bar{\rho} = 0.95$.

6. Results and discussion

We used the numerical scheme of Section 5 to compute solutions for various values of λ, h, $\bar{\varepsilon}$, E_b, τ, $\bar{c}$ and $\bar{\rho}$. The value of the undisturbed layer half-width is $\bar{d} = 1.5$, unless stated otherwise. The results presented were obtained with $N = 100$ mesh points and were checked to within graphical accuracy by varying the number of mesh points and confirming that the results were independent of N.

We begin with the case when the two unperturbed stream velocities are equal and hence $\bar{c} = 0$ in Eq. (4.16). In the limit where $\bar{\rho} \to 0$ we recover the numerical solutions of Papageorgiou and Vanden-Broeck [19], and this provides an additional check on the numerical work. Some typical nonlinear symmetric and antisymmetric profiles are shown in Figs. 3 and 4, respectively, for three representative values of the density ratio, $\bar{\rho} = 0.05, 0.5, 0.95$. The other parameters are the electric field parameter $E_b = 3$, a surface tension parameter $\tau = 1$, a permittivity ratio $\bar{\varepsilon} = 0.075$, wavelength $\lambda = 3.0$, $\bar{d} = 1$ and wave amplitude $h = 1.05$. The profiles are clearly nonlinear with rounded crests and sharp troughs. Increasing $\bar{\rho}$ has the effect of decreasing the wave steepness, for both the symmetric and antisymmetric case as is evidenced from the results. The speeds of propagation of these nonlinear waves also vary qualitatively differently (with amplitude) depending on whether the waves are symmetric or antisymmetric, as described next. It can be concluded, therefore, that in comparison with the single fluid case studied by Papageorgiou and Vanden-Broeck [19,20], the presence of the second fluid reduces the wave steepness for both symmetric and antisymmetric nonlinear waves.

In Figs. 5 and 6 we present computed values of the wave speed c versus the wave amplitude for various values of $\bar{\rho}$, for symmetric and antisymmetric waves, respectively. Starting with Fig. 5 and symmetric waves, we plot results for the density ratios $\bar{\rho} = 0.05, 0.5, 0.95$ which are represented by dashed, solid and dash-dotted lines, respectively (the same graphical representations are used in Fig. 6 also). Other parameters are $E_b = 3$, $\tau = 1$, $\lambda = 3$ and $\bar{d} = 1.5$. The corresponding linear results (see Section 3, Eqs. (3.9) and (3.10)) are represented by the straight lines superimposed on the figures, with symbols $\times$, $+$ and $*$ corresponding to $\bar{\rho} = 0.05, 0.5$ and 0.95, respectively. As noted, these are straight lines because linear theory does not account for finite amplitudes—the lines extending to order one amplitudes are simply drawn for comparison and excellent agreement is observed at small amplitudes, as expected. Several features are notable. First, for small to moderate wave amplitudes, the speeds decrease with increasing density ratio $\bar{\rho}$, in line with linear theory. Physically this is accounted for by the increasing inertial resistance to propagation induced by the enhanced presence of the outer fluid, a fact that follows directly for linear waves from the dispersion relation (3.9) (and (3.10) for antisymmetric waves). Second, for small values of the non-dimensional density ratio $\bar{\rho}$ (e.g. the results

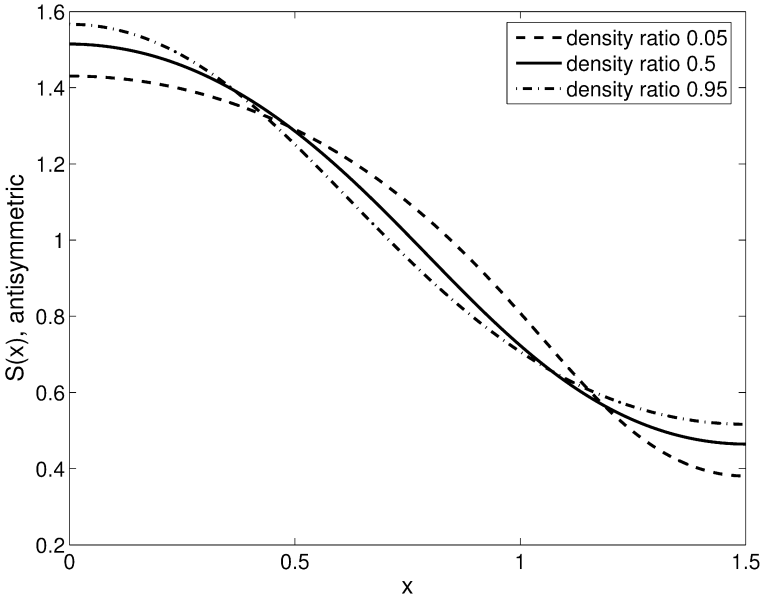

Fig. 4. Antisymmetric wave results for $E_b = 3$, $\bar{\varepsilon} = 0.075$, $\lambda = 3.0$, $h = 1.05$, $\bar{d} = 1.0$. The dashed line represents the free-surface when $\bar{\rho} = 0.05$, the solid line is for $\bar{\rho} = 0.5$ and the dash-dot line is $\bar{\rho} = 0.95$.

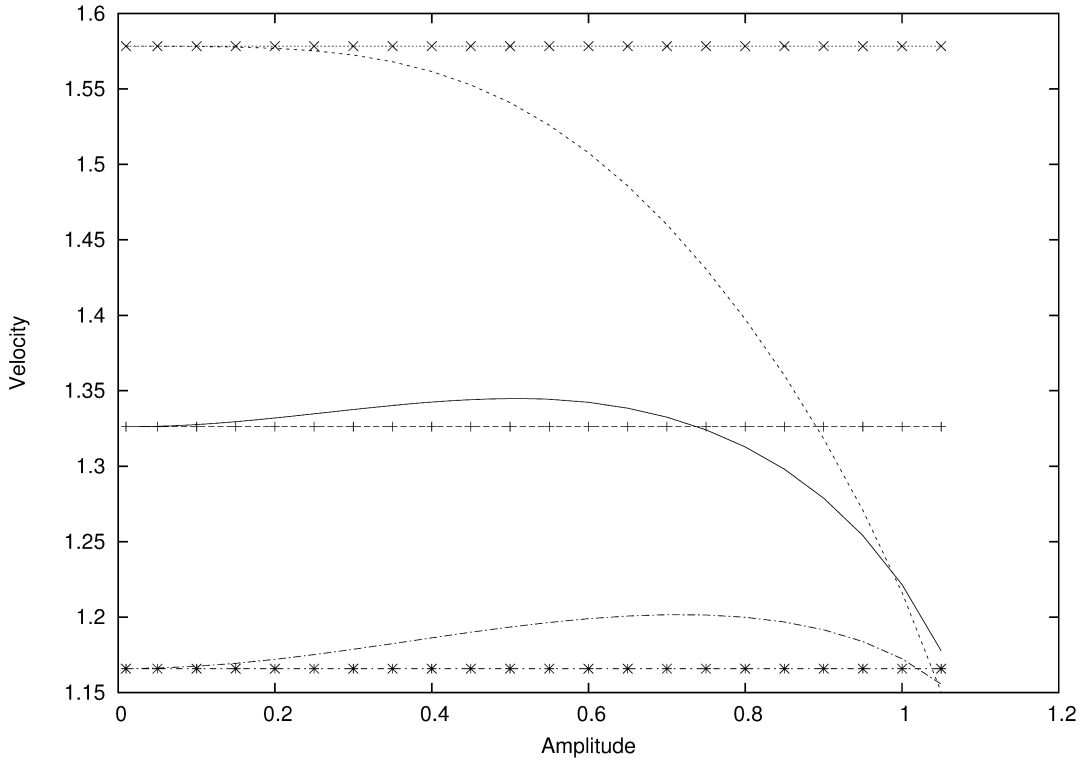

Fig. 5. Variation of wave speed with amplitude for symmetric waves; $E_b = 3$, $\bar{\varepsilon} = 0.075$, $\lambda = 3.0$, $\bar{d} = 1.5$; $\bar{\rho} = 0.05$ dashed, 0.5 solid, 0.95 dash-dot. The horizontal lines are the wave-speeds calculated from the linearized dispersion relation (3.9); $\times$, $\bar{\rho} = 0.05$; $+$, $\bar{\rho} = 0.5$; $*$, $\bar{\rho} = 0.95$.

for $\bar{\rho} = 0.05$ in Fig. 5) the wave speed c is a monotonically decreasing function of the amplitude. Such monotonic decrease in wave speed with amplitude is characteristic of symmetric waves in a single fluid system as discussed in [19]. For large values of $\bar{\rho}$ (e.g. $\bar{\rho} = 0.5$ and 0.95 in Fig. 5) the variation is no longer monotonic, but exhibits

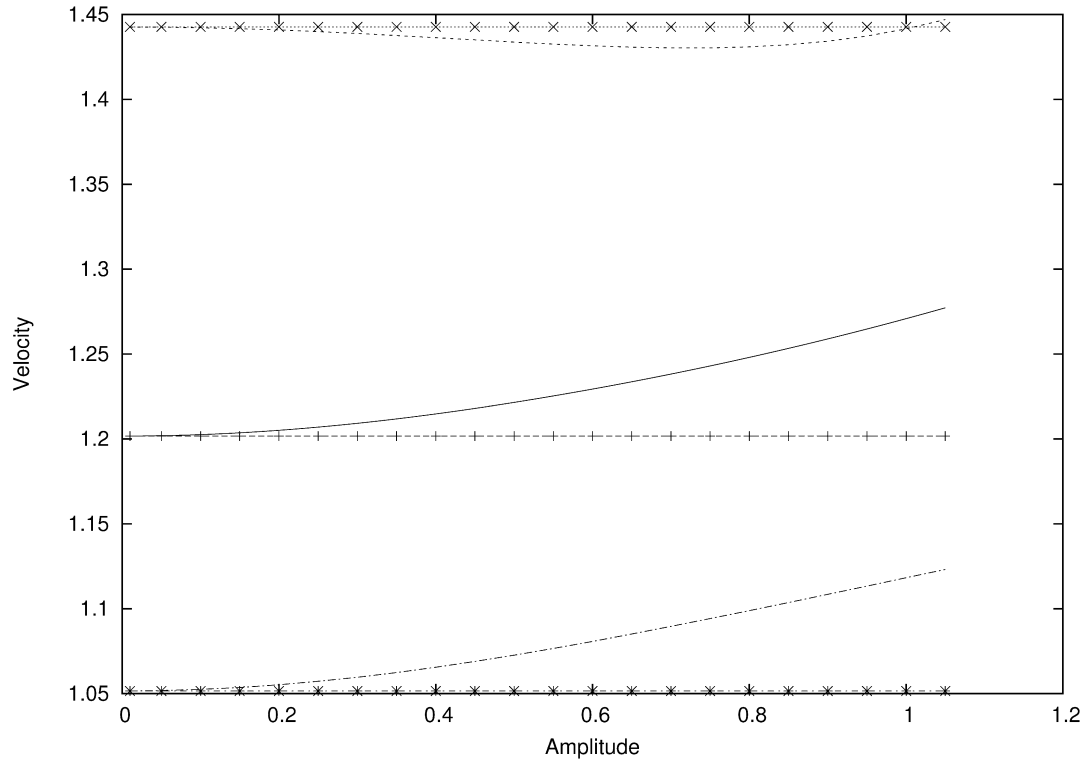

Fig. 6. Variation of wave speed with amplitude for antisymmetric waves; $E_b = 1$, $\bar{\varepsilon} = 1.5$, $\lambda = 3.0$, $\bar{d} = 1.5$, $\bar{\rho} = 0.05$ dashed, 0.5 solid, 0.95 dash-dot. The horizontal lines are the wave-speeds calculated from the linearized dispersion relation (3.10); $\times$, $\bar{\rho} = 0.05$; $+$, $\bar{\rho} = 0.5$; $*$, $\bar{\rho} = 0.95$.

a maximum at approximately $c = 0.5$ for $\bar{\rho} = 0.5$, and $c = 0.7$ for $\bar{\rho} = 0.95$—the position of the maximum shifts to higher amplitudes as $\bar{\rho}$ is increased. Through numerical calculations we estimate the transition point between monotonic decrease to monotonic increase behavior for small amplitudes, to be at a value of $\bar{\rho}$ between 0.0725 and 0.075, for this set of physical parameters. This non-monotonic behavior and the existence of a wave speed maximum, imply that for non-zero $\bar{\rho}$, nonlinear symmetric waves with amplitudes ranging between zero (linear) and some cut-off value (this value is approximately equal to 0.75 for $\bar{\rho} = 0.5$, and 1.0 for $\bar{\rho} = 0.95$), have speeds which exceed those of linear waves, whereas for amplitudes larger than these cut-off values, they lag linear waves. Note also, that due to crossing of the curves (see figure), it is possible to have two waves of the same amplitude and wave speed corresponding to different values of $\bar{\rho}$—for example, waves of amplitude approximately equal to unity corresponding to $\bar{\rho} = 0.05$ have equal speeds with those corresponding to $\bar{\rho} = 0.5$, the wave speed approximately equal to 1.23 in this example. The non-monotonic behavior discussed above is a novel feature due to the presence of a second fluid that is absent in the single fluid case studied in [19].

In Fig. 6 we present analogous results for antisymmetric waves. The parameters are the same as in Fig. 5 except for a smaller value of $E_b = 1$ and a larger permittivity ratio $\bar{\varepsilon} = 1.5$. These waves exhibit qualitatively different behavior from the symmetric case. At relatively high density ratios the wave velocity is a monotonically increasing function of amplitude (e.g. the cases $\bar{\rho} = 0.5$ and 0.95 in Fig. 6) while at relatively low density ratios there is a minimum in the wave speed—for the case $\bar{\rho} = 0.05$ included in Fig. 6, the minimum occurs at an amplitude approximately equal to 0.75. We can conclude, therefore, that antisymmetric travelling waves at low density ratios travel slower than the corresponding linear waves. Comparing with the single fluid antisymmetric waves studied in [20], we see several qualitative differences. The results of [20] show that the wave speed decreases monotonically with amplitude when $\bar{\rho} = 0$. This monotonic behavior is lost even at the very small value of $\bar{\rho} = 0.05$ as shown in Fig. 6. At larger values of $\bar{\rho}$, instead of a monotonic decrease in wave speed (and lag relative with linear speeds) we observe a monotonic increase (and larger speeds than linear ones) with amplitude, a phenomenon that is related to the presence of the outer fluid.

In Fig. 7 we present results for a non-zero velocity jump between the flows in regions 1 and 2. In particular we take $\bar{c} = 1$ in Eq. (4.16) and compute the corresponding nonlinear symmetric travelling waves in the case where $\bar{\varepsilon} = 0.075$,

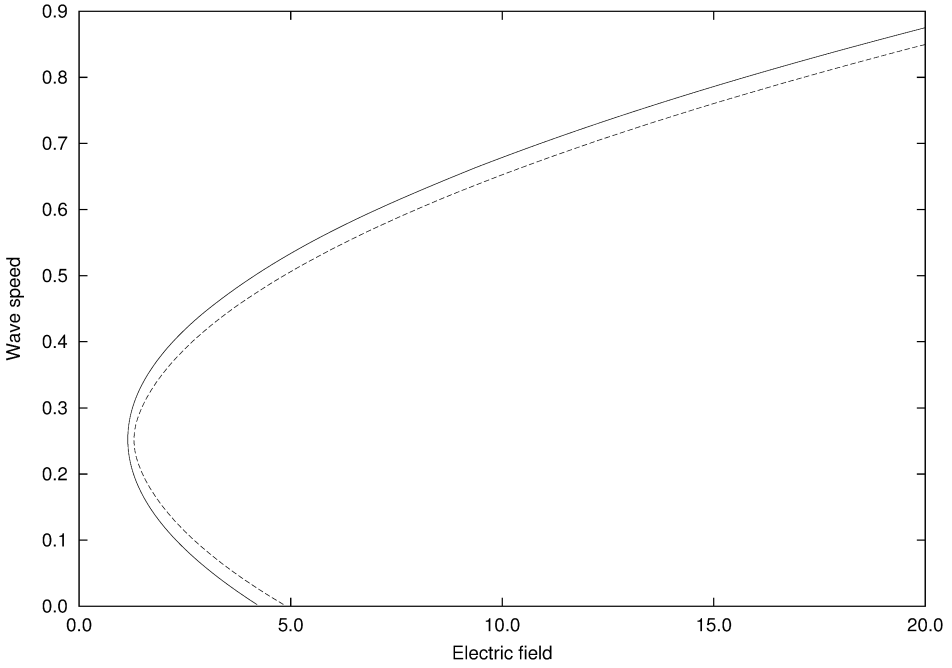

Fig. 7. Plot of the electric field parameter E_b versus wave speed for $\tau = 0$ (dashed line) and $\tau = 0.01$ (solid line).

$\bar{\rho} = 0.26$, $\lambda = 20\pi$ and $\bar{d} = 1$. The wave amplitude is taken to be $h = 0.01$. The plots represent the variation of the computed wave speed c (see Eqs. (4.14) or (4.15)) with the electric field parameter E_b for zero and non-zero ($\tau = 0.01$) surface tension—solid and dotted curves, respectively. It is evident from the results that there is a τ-dependent critical value of E_b, $E_{bc}(\tau)$ say, below which travelling waves do not exist (to the left of the "nose"). For $E_b > E_{bc}$, there are two branches of solutions, a faster (upper) and a slower (lower) branch. Upper branch solutions have increasing positive speeds whereas lower branch solutions have decreasing speeds which start off as positive but become negative above a certain value of E_b which depends on the surface tension parameter τ. We can use the linear result (3.11) to obtain the following estimate for E_{bc} (we take $k > 0$ for comparison with the computations):

$$E_{bc} = \frac{4(1+\bar{\varepsilon}\tanh kd)}{(1-\bar{\varepsilon})^2\tanh kd}\left(\frac{\bar{\rho}\bar{c}^2\tanh kd}{1+\bar{\rho}\tanh kd} - \tau k\tanh kd\right). \tag{6.1}$$

This expression reduces to the critical value given by (3.17) when $k \gg 1$. Inserting the numerical parameters of Fig. 7 into (6.1), gives a critical value of 1.194 for $\tau = 0$ and 1.189 for $\tau = 0.01$. These values are in excellent agreement with the calculations presented in Fig. 7 and this can be attributed to the relatively small wave amplitude $h = 0.01$. In their calculations of the variation of wave speeds with E_b for the symmetric case, Papageorgiou and Vanden-Broeck [19] find a monotonic increase with of c (see their Fig. 3). In the presence of an outer fluid and different stream velocities, we can see from Fig. 7 that there are two branches emanating from the critical point E_{bc}, the upper one giving a monotonic increase of c with E_b analogous to the calculations of [19], but the lower branch giving monotonically decreasing wave speeds with E_b. This additional branch is due to the presence of a second fluid and different stream velocities

7. Conclusions

In this paper we have computed arbitrary amplitude and wavelength waves on the bounding interfaces of a two-dimensional ideal fluid jet which is surrounded by a second unbounded ideal fluid of different fluid and material properties. A horizontal electric field which is uniform at infinity (laterally) acts on the system. Due to permittivity differences between the inner and outer fluids, electric Maxwell stresses enter to modify the Bernoulli equation. Four harmonic problems need to be solved, one for the fluid potential and one for the electric potential in both layers. Nonlinear interfacial conditions must also be satisfied. We have constructed boundary integral methods to compute

symmetric and antisymmetric interfacial waves (see Section 4 for definitions) of arbitrary amplitude and wavelength. This work extends that of Papageorgiou and Vanden-Broeck [19,20] by taking into account the effect of a bounding incompressible dielectric fluid upon a fluid jet in the presence of a horizontal applied electric field.

Two regimes of interest have been analyzed. The first has wave solutions whose speeds of propagation in the two fluids are equal ($\bar{c} = 0$ in the notation of Section 4). It is found that the presence of the outer fluid acts to reduce the steepness of both symmetric and antisymmetric travelling waves (see Figs. 3 and 4, respectively). The effect of the density ratio $\bar{\rho}$ (recall that this is the ratio of outer to inner density, and so the absence of a bounding fluid is characterized by $\bar{\rho} = 0$) on the speed of waves as their amplitudes increase, is more complicated. For symmetric waves, and for small values of $\bar{\rho}$, the speed decreases monotonically with amplitude (e.g. the $\bar{\rho} = 0.05$ case of Fig. 5), and nonlinear waves lag linear ones. As $\bar{\rho}$ increases, the speed-amplitude relation is no longer monotonic but increases initially with amplitude, reaches a local maximum and then decreases monotonically (e.g. the cases $\bar{\rho} = 0.5, 0.95$ of Fig. 5). The presence of the outer fluid, then, supports speeds for nonlinear waves which are faster than the corresponding linear speeds.

Antisymmetric waves behave very differently. At small enough values of $\bar{\rho}$ (e.g. the case $\bar{\rho} = 0.05$ in Fig. 6), the wave speed decreases with amplitude, reaches a local minimum and then increases monotonically. There is a range of amplitudes (starting near zero) which lag the linear waves. As $\bar{\rho}$ is increased, this behavior changes and the wave speed becomes a monotonically increasing function of amplitude—see the cases $\bar{\rho} = 0.5, 0.95$ in Fig. 4.

We have also considered the second regime where the wave speeds in the inner and outer fluid are different. Such situations are potentially susceptible to Kelvin–Helmholtz instability. Using a linear theory we have established that even in the absence of surface tension, a sufficiently strong electric field acts to stabilize Kelvin–Helmholtz instability (see Section 3.2, Eq. (3.17), for example). It is possible, then, to obtain travelling waves supporting a slip velocity at the interface, and which are stable in the sense that the linearized initial value problem is well-posed. We have computed such waves and find that for a given value of E_b larger than E_{bc} (the critical value below which the flow is Kelvin–Helmholtz ill-posed), there exist two waves of the same amplitude but of different speeds. The faster waves (upper branch) have speeds which increase monotonically with E_b, while the slower waves (lower branch) have speeds which decrease monotonically with E_b (in fact, lower branch waves attain negative speeds beyond a certain value of E_b—see Fig. 7). Inclusion of surface tension shifts the whole curve to the right due to the induced stabilization. As a result the value of E_{bc} increases as indicated in Fig. 7.

In general, then, the electric field has a dispersive effect on the jet dynamics. It is useful to consider its effect on the linear problem. If there is no outer fluid present, then the wave speed increases as E_b increases and for a fixed wavenumber the speed varies as $\sqrt{E_b}$ for large E_b. Similar behavior is found when an outer fluid is present and the inner and outer stream velocities are equal. In addition, the wave speed decreases as $\bar{\rho}$ increases, that is as the outer fluid density increases relative to that of the inner fluid. Symmetric and antisymmetric waves behave qualitatively similarly—see the dispersion relations (3.9)–(3.10). When the inner and outer stream velocities are different, short-wave Kelvin–Helmholtz instability is present. It has been shown that a sufficiently large value of E_b can completely stabilize the short-wave instability and produce waves at all wavenumbers, i.e. transforms the problem to a dispersive system. The electric field competes directly with the Kelvin–Helmholtz instability in that they have the same short-wave behavior but contribute opposite signs to the growth rate. For all the regimes discussed above we have carried out fully nonlinear computations and have constructed travelling waves of arbitrary amplitudes and wavelengths for a large range of parameters. The stability of the computed travelling waves is the subject of future work, as well as the time-dependent nonlinear evolution when a band of linearly unstable waves is present.

Finally, we discuss alternatives to surface tension regularization of Kelvin–Helmholtz instability by the addition of viscosity. At high Reynolds numbers viscous shear layers replace vortex sheets and a short wave cut-off is achieved. It would be interesting to study the fundamental problem of shear layer stability when a horizontal electric field acts; in such cases, a distribution of permittivity would need to be incorporated into the model in order to maintain different constant values at plus and minus infinity, and to address the Navier–Stokes equations linearly and nonlinearly.

Acknowledgements

This work was supported by the EPSRC grant GR/576847/01. The work of DTP was supported by the National Science Foundation Grant DMS-0072228.

References

[1] S.F. Kistler, P.M. Schweizer, Liquid Film Coating—Scientific Principles and their Technological Implications, Chapman and Hall, London, 1997.
[2] S.G. Durbin, M. Yoda, S.I. Abdel-Khalik, D.L. Sadowski, T.P. Koehler, Assessment and control of primary turbulent breakup of thick liquid sheets in IFE reactor cavities: The hydrodynamic source term, Fusion Sci. Technol. 47 (2005) 16–26.
[3] S.G. Durbin, M. Yoda, S.I. Abdel-Khalik, D.L. Sadowski, Turbulent liquid sheets for protecting IFE reactor chamber first walls, Fusion Sci. Technol. 44 (2003) 307–311.
[4] S.I. Abdel-Khalik, M. Yoda, An overview of Georgia Tech studies on the fluid dynamics aspects of liquid protection schemes for fusion reactions, Fusion Sci. Technol. 47 (2005) 601–609.
[5] N.A. Warner, Liquid metal based coal gasification, T.I. Min. Metall. C 112 (2003) C155–C176.
[6] N.A. Warner, Liquid metal systems for gasification-based power generation, P.I. Mech. Eng. A – J. Pow. 218 (2004) 387–401.
[7] D. Gallez, M. Prevost, Nonlinear rupture of thin free liquid films, J. Chem. Phys. 84 (1986) 4043–4048.
[8] R.K. Jain, C. Maldarelli, Stability of thin viscoelastic films with applications to biological membrane deformation, Ann. New York Acad. Sci. 404 (1983) 89–102.
[9] C. Maldarelli, R.K. Jain, I.B. Ivanov, E. Ruckenstein, Stability of symmetric and unsymmetric thin liquid-films to short and long wavelength perturbations, J. Colloid Interf. Sci. 78 (1980) 118–143.
[10] C. Maldarelli, R.K. Jain, The linear, hydrodynamic stability of an interfacially perturbed, transversely isotropic, thin, planar viscoelastic film. 1. General formulation and a derivation of the dispersion-equation, J. Colloid Interf. Sci. 90 (1982) 233–262.
[11] C. Maldarelli, R.K. Jain, The linear, hydrodynamic stability of an interfacially perturbed, transversely isotropic, thin, planar viscoelastic film. 2. Extension of the theory to the study of the onset of small-scale cell-membrane motions, J. Colloid Interf. Sci. 90 (1982) 263–276.
[12] M. Prevost, D. Gallez, Linear and nonlinear dynamics of free liquid films, Physicochem. Hydrodyn. 6 (1985) 731–745.
[13] G.D. Crapper, An exact solution for progressive capillary waves of arbitrary amplitude, J. Fluid Mech. 2 (1957) 532–540.
[14] L.W. Schwartz, J. Vanden-Broeck, Numerical solution of the exact equations for capillary-gravity waves, J. Fluid Mech. 94 (1979) 119–139.
[15] B. Chen, P.G. Saffman, Steady gravity-capillary waves on deep water, Stud. Appl. Math. 60 (1979) 183–210.
[16] S.J. Hogan, Some effects of surface tension on steep water waves. Part 2, J. Fluid Mech. 96 (1980) 417–445.
[17] J.K. Hunter, J. Vanden-Broeck, Solitary and periodic gravity-capillary waves of finite amplitude, J. Fluid Mech. 134 (1983) 205–219.
[18] S. Grandison, J. Vanden-Broeck, Truncation approximations for gravity-capillary free-surface flows, J. Eng. Math., in press.
[19] D.T. Papageorgiou, J.-M. Vanden-Broeck, Large-amplitude capillary waves in electrified fluid sheets, J. Fluid Mech. 508 (2004) 71–88.
[20] D.T. Papageorgiou, J.-M. Vanden-Broeck, Antisymmetric capillary waves in electrified fluid sheets, Eur. J. Appl. Math. 16 (2004) 609–623.
[21] B.S. Tilley, P.G. Petropoulos, D.T. Papageorgiou, Dynamics and rupture of planar electrified liquid sheets, Phys. Fluids 13 (2001) 3547–3563.
[22] K. Savettaseranee, D.T. Papageorgiou, P.G. Petropoulos, B.S. Tilley, The effect of electric fields on the rupture of thin viscous films by van der Waals forces, Phys. Fluids 15 (2003) 641–652.
[23] J.D. Jackson, Classical Electrodynamics, John Wiley and Sons, New York, 1963.
[24] D.T. Papageorgiou, P.G. Petropoulos, J.-M. Vanden-Broeck, Gravity capillary waves in fluid layers under normal electric fields, Phys. Rev. E 72 (2005), Art. No. 051601.
[25] R. Krasny, A study of singularity formation in a vortex sheet by the point-vortex approximation, J. Fluid Mech. 167 (1986) 65–93.